

Preparation of Hydrothermal Carbon Quantum Dots as a Contrast Amplifying Technique for the diaCEST MRI Contrast Agents

Shalini Pandey, Rimilmandrita Ghosh, and Arindam Ghosh*

Cite This: *ACS Omega* 2022, 7, 33934–33941

Read Online

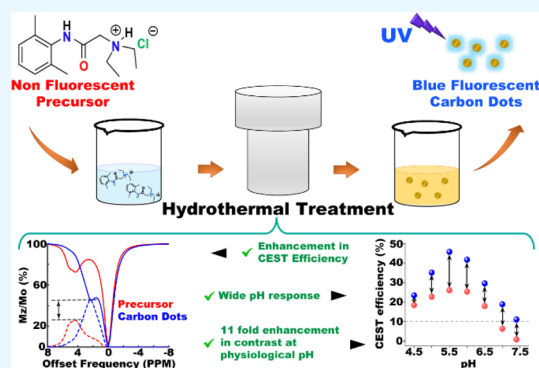
ACCESS |

Metrics & More

Article Recommendations

Supporting Information

ABSTRACT: The discovery of exogenous contrast agents (CAs) is one of the key factors behind the success and widespread acceptability of MRI as an imaging tool. To the long list of CAs, the newest addition is the chemical exchange saturation transfer (CEST)-based CAs. Among them, the diaCEST CAs are the safer metal-free option constituted by a large pool of organic and macromolecules, but the tradeoff comes in terms of smaller natural offset. Another major challenge for the CEST CAs is that they need to operate in the tens of millimolar concentration range to produce any meaningful contrast. The quest for high efficiency diaCEST agents has led to a number of strategies such as use of hydrogen bonding, use of equivalent protons, and use of diatropic ring current. Here, we present carbon quantum dot formation using hydrothermal treatment as a new strategy to amplify diaCEST contrast efficiency. We show that while the well-known analgesic drug lidocaine hydrochloride when repurposed as a diaCEST CA produces no contrast at the physiological pH and temperature, the carbon dots prepared from it elevate the physiological contrast to a sizable 11%. Also, the maximum efficiency at an acidic pH gets amplified by a factor of 2 to 46%. The study showed that the enhancement in CEST efficiency is reproducible and the pH response of these carbon dots is tunable through variation in synthesis conditions such as temperature, duration, and precursor concentration.



INTRODUCTION

Excellent spatial and temporal resolution provided by magnetic resonance imaging (MRI) along with its non-invasive nature make it one of the most successful diagnostic imaging techniques for soft tissues.¹ While there exist techniques for in vivo imaging that provide superior sensitivity such as positron emission tomography, they often lack in resolution.² Optical imaging methods on the other hand suffer from poor in-depth penetration. The widespread popularity of MRI can be attributed to a large extent to the discovery of exogenous contrast agents (CAs).^{3,4} These are small molecules that create artificial contrast between the area of investigation and the surrounding by selectively altering the water signal intensity. Thus far, all the CAs approved for clinical usages are relaxation-based ones, which either alter the T_1 or the T_2 of water in the proximity.^{4,5} The relaxation-based CAs have, however, reservations of their own—the most important one being that contrast cannot be turned-off once administered. Also, the long term safety⁶ is a matter of debate for the relaxation-based CAs which are mostly gadolinium (III)-based chelates.⁷ In 2000, chemical exchange saturation transfer (CEST) was utilized as an alternative MR imaging contrast generation technique in order to address the limited sensitivity, switchability, and safety of CAs.⁸ CEST CAs alter water intensity by transferring saturation to the accessible water through chemical exchange after being selectively saturated by the application of a long low-power radio-frequency pulse train.^{9,10} As the contrast is generated only

when the solute exchangeable proton pool is first selectively saturated, it becomes rather straight forward to either turn-on or turn-off the contrast. However, the requirement of selective saturation of the solute demands that the solute exchangeable protons resonate far from water protons. A class of CEST CAs known as the paraCEST CAs excels in creating large offsets ($\Delta\omega$) due the presence of a paramagnetic metal center ligated with multi-dentate ligands.^{9,11} A large offset helps in two more ways. First, it helps to avoid overlapping with almost all endogenous exchangeable protons present inside the body. Second, a large offset allows protons with relatively higher exchange rates (k_{ex}) to produce contrast remaining in the slow to medium exchange regime ($k_{ex} \leq \Delta\omega$).¹² A larger k_{ex} then in turn produces high efficiency (larger contrast).

diaCEST CAs,¹³ on the other hand, do not contain any metal and hence are considered a safer alternative. However, they suffer heavily both in terms of offset and efficiency. The quest for efficient diaCEST CA has prompted testing of almost all classes of organic compounds containing labile protons in the slow to

Received: May 10, 2022

Accepted: August 30, 2022

Published: September 12, 2022



medium exchange regime, including endogenous CAs such as glucose,¹⁴ glycogens,¹⁵ glycosaminoglycan,¹⁶ protamine,¹⁷ glutamate,¹⁸ urea,¹⁹ nucleic acids,²⁰ peptides,²¹ and so forth present inside the human body. Few of the already known clinical agents have also been repurposed as diaCEST CAs.^{22,23} However, even then the sensitivity or efficiency of diaCEST CAs remains an ongoing challenge.

The efficiency of CEST CAs depends, in an intertwined manner, on a number of molecular properties such as the optimality of exchange rate, offset from water, and availability of more than one equivalent exchangeable protons. A synergy between these factors produces the most efficient diaCEST agents. For example, salicylic acid²⁴ not only gains from a large down-field offset of ~9 ppm, it belongs to a group of compounds in which either intramolecular²⁵ or intermolecular^{22,26} hydrogen bonding slows down the exchange rate so optimally that the contrast efficiency increases. On the other hand, few porphyrin derivatives²⁷ along with a large up-field shift of almost -8 ppm benefit from two equivalent exchangeable protons similar to iopamidol,²⁸ and certain polymers,²⁹ thereby naturally producing good contrast. Finally, a few diacetamide derivatives²⁶ exploit the benefit from both equivalent exchangeable protons and finely tuned exchange rates through intermolecular hydrogen bonding. Nonetheless, a diaCEST CA would still require tens of millimolar concentration to produce any meaningful contrast. The problem is further compounded by poor water solubility of a few compounds requiring prohibited quantity of material to be injected.

Here, we present conversion to water-soluble carbon quantum dots (CDs) as a strategy to address together the low efficiency and solubility problems of diaCEST CAs. Nanoparticles are not new to the world of medicine³⁰ and imaging.³¹ Among different nano-particles, CDs have recently gained tremendous popularity as they are cost effective, generally safer than many other metal-containing nano-particles, highly fluorescent, and many of them show better water solubility than their respective precursors.³² In 2019, an arginine-modified glucose-based CD was introduced as a new class of diaCEST CAs by Liu's group.³³ Their microwave-synthesized CDs showed good contrast at physiological pH owing to the presence of both hydroxyl and guanidinium groups on the surface. As amides form the basic block of several diaCEST CAs, we chose to test if some amide group-containing molecule shows enhancement in diaCEST efficiency post CD formation. For the current study, we selected Lidocaine hydrochloride (L-HCl for brevity), a clinically approved analgesic drug that hitherto has not been reported as a diaCEST CA. We employed hydrothermal treatment for CD formation. We show that while L-HCl does not produce any contrast (<1%) at the physiological condition (pH 7.4, 37 °C), the L-HCl CD shows a good 11% contrast at the same concentration. Also, the peak efficiency of L-HCl gets amplified by almost 100% upon formation of CD.

METHODS AND MATERIALS

Instrumentation and Materials. All NMR experiments for preparation of Z-spectra were performed at 310 K using a BBFO broadband probe on a 9.4 T (400 MHz) Bruker AVANCE-III Nanobay NMR spectrometer. All ¹H and ¹³C spectra were recorded at 298 K using a Bruker 700 MHz (16.4T) Avance-III HD liquid-state NMR spectrometer equipped with a triple-channel cryoprobe with z-gradients. D₂O-filled capillaries were placed inside the NMR tubes for achieving deuterium lock. A Jasco V-730 spectrophotometer was used to record the steady-

state absorption spectra. The emission spectra were recorded on a Shimadzu RF-6000 fluorescence spectrophotometer. High resolution TEM (HR-TEM) images were captured using a JEOL (JEM-2100, 200 kV) electron microscope.

Synthesis of Carbon Dots. L-HCl-based carbon dots were synthesized using the hydrothermal method under variable conditions starting from different precursor concentrations. 2.5 and 5 mg/mL stock aqueous solutions of L-HCl were prepared by dissolving, respectively, 250 and 500 mg of compound into 100 mL of deionized water. The mixtures were subjected to a rotary-shaker until clear colorless solutions were obtained. Each of the solutions was then placed inside a hot air oven after separately taken and transferred to a teflon-lined steel autoclave reactor of 50 mL capacity. With the 2.5 mg/mL stock, two CDs were prepared at 200 °C with different treatment durations—one for 24 h, and the other for 10 h. The 5 mg/mL stock, on the other hand, was subjected to hydrothermal treatment for three different temperature-duration pairs: (200 °C, 10 h), (200 °C, 24 h), and (180 °C, 24 h). Certain portions of the stock solutions were kept aside for experiments as reference compound and for comparison. After the solution went through their respective stipulated treatments, the autoclave was taken out of the oven and was allowed to cool down at room temperature. The resulting clear solutions showed different shades of yellow. The change of color acted as an indicator for the formation of the CDs. The color changed the least for the treatment at 180 °C. Each sample was passed through sterilized 0.2 μm chromatography filter to ensure the removal of all suspended large particles. The CD solutions showed blue to cyan characteristic fluorescence upon subjecting to UV light.

Preparation of CEST Z-Spectra. CEST experiments were performed with selective solute saturation at a resolution of 0.25 ppm between offsets -8 and 8 ppm with respect to the water. Irradiation radiofrequency of 213 Hz (5 μT) field strength was used for the saturation duration of 3 s. The saturation duration and irradiation frequency were kept constant throughout to facilitate better comparison of different compounds. Z-spectra were generated by plotting the normalized water peak intensity ($100 \times M_z/M_0$) as a function of irradiation offset frequency, where M_z and M_0 are the water peak intensities with and without on-resonance selective saturation. CEST contrast efficiency was given by the asymmetric magnetization transfer ratio (MTR_{assym})¹²

$$\text{CEST efficiency} = \frac{M(-\Delta\omega) - M(\Delta\omega)}{M(\Delta\omega)} \times 100\%$$

$M(\Delta\omega)$ and $M(-\Delta\omega)$ are water peak intensities, respectively, after saturation at the site of the exchangeable peak (offset $\Delta\omega$) and saturation at a negative offset (offset $-\Delta\omega$) present on the other side of the water peak. All post-acquisition processing and plotting were done using in-house MATLAB (R2014b) scripts.

Exchange Rate Calculation. Exchange rate calculations were performed using a method introduced by Dixon et al. in which the value of $M_z/(M_0 - M_z)$ is linearly fitted against $1/\omega_1^2$ from a set of Z-spectra acquired with variable saturation fields. The linear fit gives the value of exchange rate k_{ex} when the x -axis intercept is equated to $-1/(k_{\text{ex}}^2)$.³⁴ ω_1 is given by γB_1 , where γ is the gyromagnetic ratio of proton and B_1 is the r.f. amplitude. This method requires conditions such as minimal water direct saturation (DS), saturation power less than the offset $\Delta\omega$ (both in Hz), and a saturation duration long enough for complete saturation. To fulfil these criteria, a long saturation duration of 6

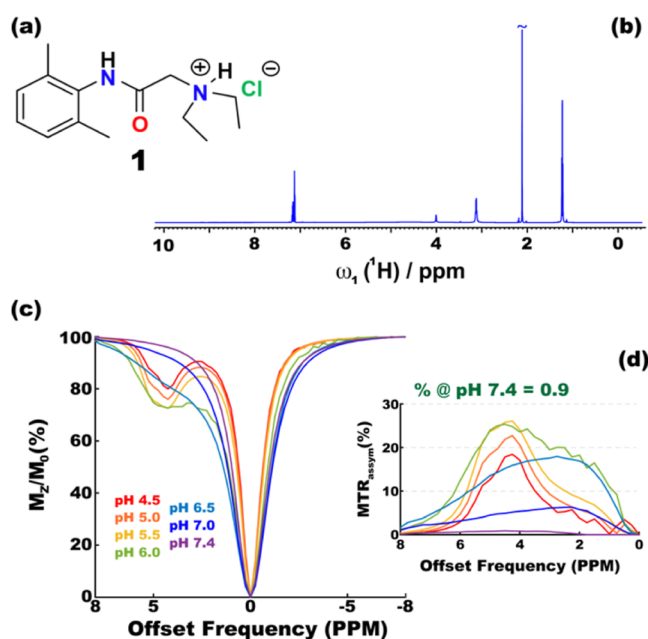


Figure 1. Characterization and CEST profiles of lidocaine hydrochloride: (a) structure and (b) ^1H ^1D -NMR spectrum in water. (c) Z-spectra and (d) $\text{MTR}_{\text{asymp}}$ as a function of pH of the solution in the range from pH 4.5 to pH 7.4. CEST efficiency at the physiological pH (7.4) is specifically mentioned.

s and low direct saturation producing Sinc pulse-train were used. Taking $\Delta\omega$ of the compound into account, maximum saturation powers were adjusted. All fittings and plotting were done using in-house codes in MATLAB 2014b.

RESULTS AND DISCUSSION

Lidocaine Hydrochloride as a diaCEST CA. Lidocaine is an amphiphilic compound generally used as a local anaesthetic either as a topical solution or in the injection form. It contains an amide group adjacent to a phenyl ring. The diatropic ring current produces a useful down-field shift ($\Delta\omega = \sim 4.5$ ppm with respect to water) for the amide proton, making it suitable for CEST contrast generation. Additionally, it contains a terminal tertiary amine group, which also shows diaCEST contrast when protonated. As the protonated form of local anaesthetics has better stability and solubility than its free base, the hydrochloride salt form is used in almost all medicinal applications.³⁵ The white crystalline L-HCl salt (**1** in Figure 1a) is highly water-soluble and exists in the monohydrate form. Figure 1b shows the ^1H NMR spectrum of **1** in water (Figure S1 for ^{13}C spectrum). The exchangeable protons are exchange-broadened and are missing. A 5 mg/mL aqueous solution (17 mM) of **1** produces appreciable CEST contrast in a wide acidic pH range between pH 4.5 and pH 7.0 (Figure 1c), reaching a maximum efficiency of 26.1% at pH 5.5. The $\text{MTR}_{\text{asymp}}$ plots (Figure 1d) show interesting features of **1**. While around neutral pH (up to pH 6.5) the quaternary ammonium group Et_3NH^+ predominantly showed CEST at around 2.25 ppm downfield to water, the CEST peak slowly moved to 4.25 ppm in the acidic pH range when the amide protons (-CONH) started exchanging with water. At a very acidic pH (below pH 5), the amide proton of course stopped exchanging and the overall CEST efficiency rapidly dropped. In spite of the fact that **1** has been proven safe, is easily soluble in water, and produces an appreciable 26% CEST contrast at pH 5.5, the lack of contrast at the serum physiological pH makes it unsuitable as a general purpose CA. We now show how CD formation by hydrothermal treatment of **1** helps to tune the CEST properties more toward a favorable pH

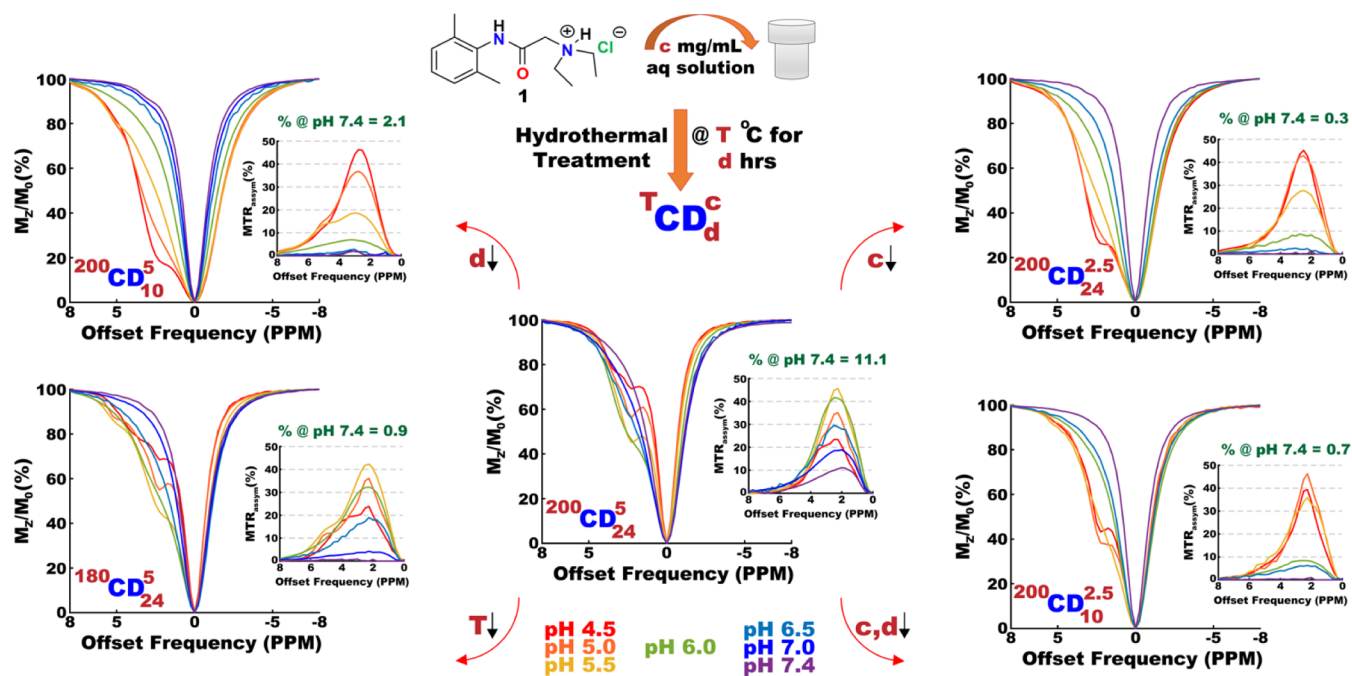


Figure 2. One-pot hydrothermal synthesis of carbon quantum dots from lidocaine hydrochloride and their CEST profiles as a function of pH: Carbon dot synthesized by hydrothermal treatment of “c” mg/mL solution of the precursor at temperature “T” for “d” hours is denoted as $^T\text{CD}_d^c$. The inset of each z-spectrum shows the corresponding $\text{MTR}_{\text{asymp}}$ (CEST efficiency). $^{200}\text{CD}_5^{24}$ (center) shows the maximum contrast at serum physiological pH 7.4 and temperature 37°C (indicated over $\text{MTR}_{\text{asymp}}$ plots). Lowering (denoted by the down arrow) of values for any of the synthesis conditions from that set caused the physiological contrast to drop.

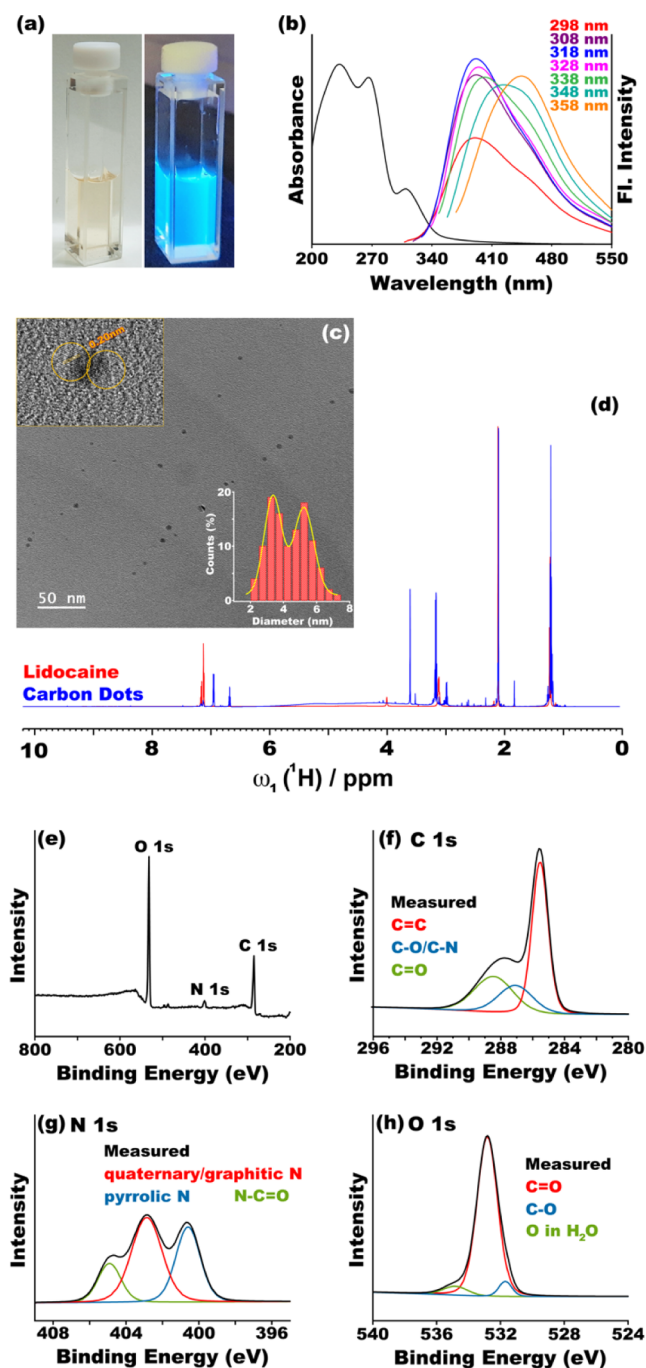


Figure 3. Characterization of $^{200}\text{CD}_{24}^5$: (a) solution under visible and UV illumination. (b) Absorption and emission spectra. (c) TEM image of the carbon dots. Top inset: crystal line spacing (0.2 nm). Bottom inset: particle size distribution with double Gaussian fitting. Mean particle size: $\mu_1 = 3.4$ nm, $\sigma_1 = 0.55$ nm and $\mu_2 = 5.2$ nm, $\sigma_2 = 0.65$ nm (d) comparison of ^1H 1D-NMR spectra of **1** (red) with that of $^{200}\text{CD}_{24}^5$ (blue). NMR, absorption, and emission spectra of other CDs are given in Figures S2–S13. (e) XPS spectrum with the expansions of C 1s (f), N 1s (g), and O 1s (h) regions.

range and produces an overall enhancement of the contrast efficiency. We also show how different conditions during the hydrothermal treatment such as precursor concentration (c in mg/mL), temperature (T in $^\circ\text{C}$), and duration (d in hours) can be used as individual tuning parameters for optimization of the CEST contrast profile of the CDs. Carbon dots prepared by

hydrothermal treatment of “ c ” mg/mL solution of **1** at “ T ” $^\circ\text{C}$ for “ d ” hours would be denoted as $^T\text{CD}_c^d$.

Optimization of Hydrothermal Synthesis Conditions.

Condition tuning led us to the most favorable carbon dot formation with highest physiological contrast when we used 5 mg/mL aqueous solution of **1** and treated it at 200 $^\circ\text{C}$ for 24 h ($^{200}\text{CD}_{24}^5$, Figure 2-center). The maximum efficiency of $^{200}\text{CD}_{24}^5$ reached nearly double of that of **1** (45.7% at pH 5.5). More importantly, the efficiency at the physiological condition showed a good 11% from nearly no contrast (<1%) by **1**. From this favorable parameter set, when we varied the duration ($^{200}\text{CD}_{10}^5$, Figure 2-top left), the temperature ($^{180}\text{CD}_{24}^5$, Figure 2-bottom left), the concentration ($^{200}\text{CD}_{24}^{2.5}$, Figure 2-top right), and the concentration–duration pair ($^{200}\text{CD}_{10}^{2.5}$, Figure 2-bottom right), we found that the physiological contrast dropped drastically back to near zero. Among the three conditions, we found that duration and concentration have more drastic effects on the pH profile than temperature. Both $^{200}\text{CD}_{10}^5$ and $^{200}\text{CD}_{24}^{2.5}$ show contrast 10% or more only at pH 5.5 or below. On the contrary, $^{180}\text{CD}_{24}^5$ showed nearly 20% contrast even at pH 6.5. Overall, the CD synthesis conditions turned out to be extremely sensitive tuning parameters for the pH profile of the contrast. Despite the differences, the CDs showed some common features too. First, the peak efficiency for all of the CDs remained around 45% ensuring a consistent enhancement in efficiency over the precursor **1**. Second, the CEST MTR_{asym} plot for all the CDs showed a sharp rise around the offset 2.25 ppm with an asymmetric slow decaying tail toward higher offset. While the sharp primary CEST peak is coming from the protonated tertiary amine group, the asymmetry is arising most likely due to a small contribution from the amide proton at the offset 4.25 ppm. It is rather expected that the amide protons would not participate in CEST much as the bulky terminal amine group on the surface of the CDs would restrict the solvent access for the amide protons placed closer to the phenyl ring and hence to the core of the CD.

Characterization of $^{200}\text{CD}_{24}^5$. After establishing that $^{200}\text{CD}_{24}^5$ gives the best contrast at serum physiological condition, we went onto characterizing it and performing in-depth comparison with its precursor. To start with, post CD formation, the color of the solution changed to pale yellow from a colorless solution of **1**. No precipitation or turbidity was observed over a long period of time. $^{200}\text{CD}_{24}^5$ showed blue fluorescence under UV light (Figure 3a). The absorbance and emission spectra further confirmed the fluorescence properties in the carbon dot solution (Figure 3b). As observed for most CDs, the emission maximum of $^{200}\text{CD}_{24}^5$ also showed a distinct redshift with increasing excitation wavelength. Blue fluorescence is generally produced by relatively smaller size CDs.³⁶ TEM confirmed that the size distribution has two peaks (Figure 3c). One at 3.4 nm ($\sigma = 0.55$ nm), and the other at 5.2 nm ($\sigma = 0.65$ nm). These dot sizes are consistent with the typical blue emission. The crystal lines had a spacing of 0.20 nm as shown in the inset of Figure 3c. The ^1H NMR spectrum of $^{200}\text{CD}_{24}^5$ showed significant peak shifts in the aromatic region as compared to the aliphatic region (Figure 3d). This indicates that while the phenyl rings participate in the core formation (change of environment leading to change in chemical shifts), the environment of the side chain functional groups on the surface of the CDs, especially the tertiary amine group, remains intact. The structural changes were further confirmed by the ^{13}C spectrum (Figure S14). X-ray photoelectron spectroscopy (XPS) measurements gave further insights toward the doping and surface groups. The wide-scan

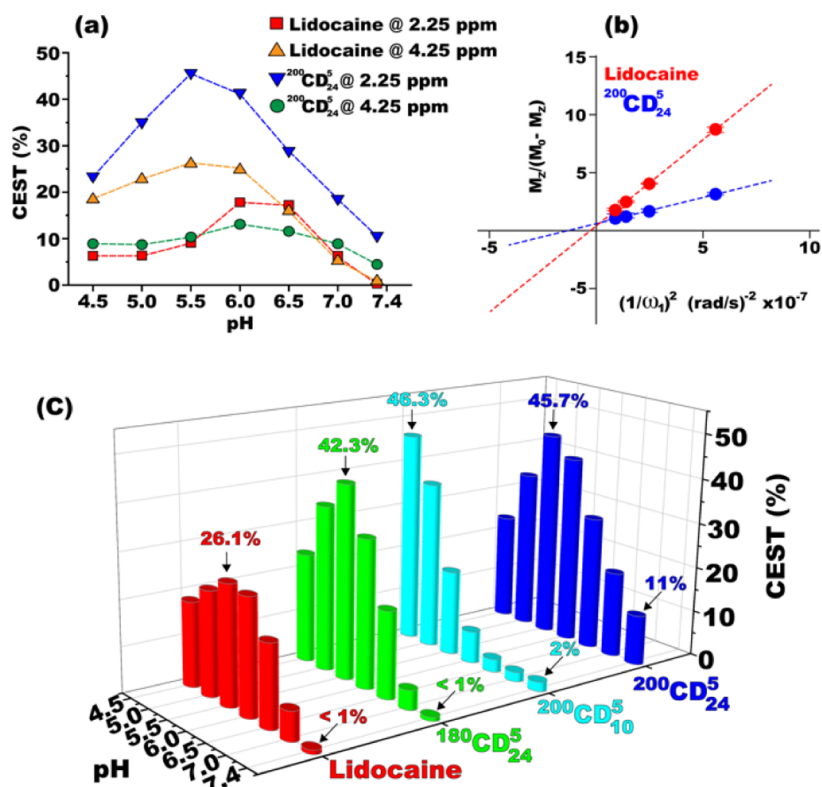


Figure 4. Comparison of pH response of CEST efficiency and exchange coefficient for **1** and CDs: (a) CEST efficiency of amide (measured at 4.25 ppm offset) and tertiary amine (2.25 ppm) protons as a function of pH. (b) Linear regression of $M_z/(M_z - M_0)$ against $1/\omega^2$ for calculating k_{ex} of **1** (red) and ²⁰⁰CD₂₄ (blue). (c) Highest CEST efficiency shown by **1** and three other CDs irrespective of offsets.

XPS spectrum of ²⁰⁰CD₂₄ shown in Figure 3e clearly shows three peaks corresponding to C 1s, N 1s, and O 1s, respectively, around 285, 402, and 532.0 eV. A distinctive peak for N 1s confirms the nitrogen doping into the carbon dots. Deconvolution of the C 1s peak in Figure 3f shows peaks centered at 285.5, 287.1, and 288.5 eV, respectively, corresponding to C=C, C-O/C-N, and C=O groups. Figure 3g shows that the N 1s peak can be constructed by three components corresponding to pyrrolic N, graphitic/quaternary N, and amide N (N-C=O), respectively, at 400.6, 402.86, and 404.9 eV. A high resolution O 1s spectrum (Figure 3h) was fitted with three peaks. While the peaks at 531.7 and 532.8 eV correspond to, respectively, C-O and C=O, the small peak at 534.8 eV is attributed to O present in H₂O. The presence of protonated tertiary amine and carbonyl groups was further confirmed by peaks at 2360 and 1630 cm⁻¹ in the IR spectrum of ²⁰⁰CD₂₄ (Figure S15).

Exchange Constant Measurement and Comparison. In order to find a possible explanation behind the fact that hydrothermal treatment amplifies the CEST efficiency in all the reaction conditions that were tried, we decided to measure exchange constants (k_{ex}) of both the precursor (**1**) and the ²⁰⁰CD₂₄. To start with, we plotted and compared the CEST efficiencies of both the compounds as a function of pH at two offsets: 2.25 ppm for the protonated tertiary amine group and 4.25 ppm for the amide proton. This was to find a common pH where both compounds give enough CEST at a particular frequency, so that k_{ex} can reliably be measured and compared for any one type of proton. As seen from Figure 4a, both compounds give maximum contrast at pH 5.5, but ²⁰⁰CD₂₄ gives it at 2.25 ppm offset (blue inverted triangle) and **1** gives at 4.25 ppm (yellow triangle) offset. Therefore, a k_{ex} measurement at pH 5.5

would compare two different functional groups. Fortunately, both compounds show enough CEST efficiency at 2.25 ppm (red square and blue inverted triangle) around pH 6–6.5, so that k_{ex} of the protonated tertiary amine group can be measured and compared reliably. We chose pH 6.5 for our k_{ex} study as it is closer to the neutral pH. Figure 4b shows the linear fitting of $M_z/(M_z - M_0)$ against $1/\omega^2$ for **1** (red) and ²⁰⁰CD₂₄ (blue). Clearly, the slope is much higher, and hence, the x-axis intercept for **1** (corresponding to a higher k_{ex} of 6080 rad s⁻¹) is much smaller than that of ²⁰⁰CD₂₄ (blue, k_{ex} of 2750 rad s⁻¹). We believe that the drop of k_{ex} to a more suitable value post hydrothermal treatment is one of the major factors leading to the enhancement of CEST efficiency. For a small offset of 2–4 ppm, a k_{ex} of 6080 rad s⁻¹ for **1** is rather high, leading to ineffective saturation transfer.

CEST Comparison of CDs and Their Precursor. As the precursor and its CDs give maximum CEST at different offsets (Figure 4a) and also different CDs give slightly different profiles (Figure 2), comparison of CEST efficiency at any particular frequency either at 2.25 or at 4.25 ppm does not do justice to any of them. To capture a true comparison, we plotted the pH dependence of highest CEST efficiencies, irrespective of offsets, for various samples having the same concentration (5 mg/mL): **1**, ¹⁸⁰CD₂₄, ²⁰⁰CD₁₀, and ²⁰⁰CD₂₄ (Figure 4c). Clearly, the pH response and efficiency of a compound can be very different post hydrothermal treatment. More importantly, the synthesis conditions can be used for further fine tuning of the pH profiles. Among all the CDs, ²⁰⁰CD₁₀ gives the highest CEST at 46.3% but only at a highly acidic pH of 4.5. The other two CDs sport a similar pH profile (peaking at pH 5.5) in comparison to **1**, but only ²⁰⁰CD₂₄ gives any meaningful contrast at the medically important neutral and physiological pH. Overall, increasing the

temperature and duration enhanced the physiological contrast ($^{180}\text{CD}_{24}^5 < ^{200}\text{CD}_{10}^5 < ^{200}\text{CD}_{24}^5$).

CONCLUSIONS

The key challenge of CEST CAs is their inherent insensitivity. For diaCEST agents, the problem is compounded by the low offsets of the exchangeable protons with respect to water as the protons having a slightly larger exchange constant cease to produce good contrast. A number of strategies have been tried and tested to overcome the sensitivity issue. Among them, use of equivalent exchangeable protons, use of inter- and intramolecular hydrogen bonding as a control over the exchange constant, and searching for natural high offset molecules have shown great success in recent times. Here, we present a new strategy in the form of converting a compound to carbon quantum dots (CDs) using hydrothermal treatment. We demonstrate that CDs show large amplification of CEST efficiency in comparison to its precursor at the same concentration. Moreover, different hydrothermal synthesis conditions such as precursor concentration, reaction temperature, and reaction time work as tuning parameters for the pH response of the resulting CDs. In the current study, we have first repurposed a well-known analgesic drug lidocaine hydrochloride as a diaCEST CA. While it showed very good CEST (~26%) contrast predominantly in the acidic pH, the efficiency dropped drastically below 1% at the all-important physiological pH and temperature. We demonstrated that in the most optimized conditions, the carbon dots amplify the physiological efficiency several folds to 11% and the overall efficiency by a factor of nearly 2 to 46%. The one-pot synthesis was easy to perform, and the amplification was reproducible across batches. Also, the formation of CDs makes the CEST peak sharper as opposed to the wide profile produced by the precursor, facilitating a better exploitation of dose administered. In the quest of finding a plausible explanation for the impressive amplification in contrast efficiency shown by the CDs, we measured the exchange constants (k_{ex}) of both the precursor and the CDs. We found that the k_{ex} of the CDs is better suited for a small offset of the exchangeable protons leading to a better efficiency. However, the suitability of exchange constant is perhaps just one of many factors and other factors such as some inherent property of CDs cannot be ruled out. It becomes therefore important that further investigation of CDs as CEST CAs continues. Overall, through this study, we show that carbon dots as diaCEST agents have great potential that needs immediate exploration.

ASSOCIATED CONTENT

Supporting Information

The Supporting Information is available free of charge at <https://pubs.acs.org/doi/10.1021/acsomega.2c02911>.

^{13}C NMR spectrum of the precursor and additional characterization spectra and plots ($^1\text{H}/^{13}\text{C}$ NMR, absorption spectrum, emission spectrum, and IR spectrum) for the carbon dots (PDF)

AUTHOR INFORMATION

Corresponding Author

Arindam Ghosh – School of Chemical Sciences, National Institute of Science Education and Research Bhubaneswar (NISER), HBNI, Khordha 752050 Odisha, India; orcid.org/0000-0002-6963-9879; Email: aringh@niser.ac.in

Authors

Shalini Pandey – School of Chemical Sciences, National Institute of Science Education and Research Bhubaneswar (NISER), HBNI, Khordha 752050 Odisha, India; orcid.org/0000-0003-0604-2079

Rimilmandrita Ghosh – School of Chemical Sciences, National Institute of Science Education and Research Bhubaneswar (NISER), HBNI, Khordha 752050 Odisha, India

Complete contact information is available at:

<https://pubs.acs.org/10.1021/acsomega.2c02911>

Author Contributions

S.P. conceptualized the project and prepared the carbon dots. S.P. and R.G. performed all the experiments and analyzed data using in-house MATLAB codes written by A.G. Overall supervision and manuscript drafting were done by A.G.

Notes

The authors declare no competing financial interest.

ACKNOWLEDGMENTS

We thank NISER and DAE, India for the infrastructure. S.P. thanks NISER and DAE for financial support. A.G. and S.P. thank Dr. Sudip Barman for his suggestions and help. The use of the central instrument facilities at NISER, Bhubaneswar, and at IISc, Bengaluru, is acknowledged.

REFERENCES

- (1) Slavin, G. S.; Bluemke, D. A. Spatial and Temporal Resolution in Cardiovascular MR Imaging: Review and Recommendations. *Radiology* **2005**, *234*, 330–338.
- (2) Vaquero, J. J.; Kinahan, P. Positron Emission Tomography: Current Challenges and Opportunities for Technological Advances in Clinical and Preclinical Imaging Systems. *Annu. Rev. Biomed. Eng.* **2015**, *17*, 385–414.
- (3) (a) Galdes, C. F. G. C.; Laurent, S. Classification and basic properties of contrast agents for magnetic resonance imaging. *Contrast Media Mol. Imaging* **2009**, *4*, 1–23. (b) Xiao, Y.-D.; Paudel, R.; Liu, J.; Ma, C.; Zhang, Z.-S.; Zhou, S.-K. MRI contrast agents: Classification and application (Review). *Int. J. Mol. Med.* **2016**, *38*, 1319–1326. (c) Gao, M.; Shen, B.; Zhou, J.; Kapre, R.; Louie, A. Y.; Shaw, J. T. Synthesis and Comparative Evaluation of Photoswitchable Magnetic Resonance Imaging Contrast Agents. *ACS Omega* **2020**, *5*, 14759–14766.
- (4) (a) Young, I. R.; Clarke, G. J.; Baffles, D. R.; Pennock, J. M.; Doyle, F. H.; Bydder, G. M. Enhancement of relaxation rate with paramagnetic contrast agents in NMR imaging. *J. Comput. Tomogr.* **1981**, *5*, 543–547. (b) Hingorani, D. V.; Bernstein, A. S.; Pagel, M. D. A review of responsive MRI contrast agents: 2005–2014. *Contrast Media Mol. Imaging* **2015**, *10*, 245–265.
- (5) (a) De León-Rodríguez, L. M.; Martins, A. F.; Pinho, M. C.; Rofsky, N. M.; Sherry, A. D. Basic MR relaxation mechanisms and contrast agent design. *Journal of magnetic resonance imaging: JMIR* **2015**, *42*, 545–565. (b) Lauffer, R. B. Paramagnetic metal complexes as water proton relaxation agents for NMR imaging: theory and design. *Chem. Rev.* **1987**, *87*, 901–927.
- (6) Rydahl, C.; Thomsen, H. S.; Marckmann, P. High Prevalence of Nephrogenic Fibrosis in Chronic Renal Failure Patients Exposed to Gadodiamide, a Gadolinium-Containing Magnetic Resonance Contrast Agent. *Invest. Radiol.* **2008**, *43*, 141–144.
- (7) (a) Wahsner, J.; Gale, E. M.; Rodríguez-Rodríguez, A.; Caravan, P. Chemistry of MRI Contrast Agents: Current Challenges and New Frontiers. *Chem. Rev.* **2019**, *119*, 957–1057. (b) Aime, S.; Botta, M.; Fasano, M.; Terreno, E. Lanthanide(III) chelates for NMR biomedical applications. *Chem. Soc. Rev.* **1998**, *27*, 19–29.

- (8) Ward, K. M.; Balaban, R. S. Determination of pH using water protons and chemical exchange dependent saturation transfer (CEST). *Magn. Reson. Med.* **2000**, *44*, 799–802.
- (9) Viswanathan, S.; Kovacs, Z.; Green, K. N.; Ratnakar, S. J.; Sherry, A. D. Alternatives to gadolinium-based metal chelates for magnetic resonance imaging. *Chem. Rev.* **2010**, *110*, 2960–3018.
- (10) van Zijl, P. C. M.; Yadav, N. N. Chemical exchange saturation transfer (CEST): What is in a name and what isn't? *Magn. Reson. Med.* **2011**, *65*, 927–948.
- (11) (a) Burns, P. J.; Cox, J. M.; Morrow, J. R. Imidazole-Appended Macrocyclic Complexes of Fe(II), Co(II), and Ni(II) as ParaCEST Agents. *Inorg. Chem.* **2017**, *56*, 4545–4554. (b) Hancu, I.; Dixon, W. T.; Woods, M.; Vinogradov, E.; Sherry, A. D.; Lenkinski, R. E. CEST and PARACEST MR contrast agents. *Acta Radiol.* **2010**, *51*, 910–923. (c) Tsitovich, P. B.; Cox, J. M.; Sperry, J. A.; Morrow, J. R. Gear Up for a pH Shift: A Responsive Iron(II) 2-Amino-6-picolyl-Appended Macrocyclic paraCEST Agent That Protonates at a Pendent Group. *Inorg. Chem.* **2016**, *55*, 12001–12010. (d) Woods, M.; Woessner, D. E.; Sherry, A. D. Paramagnetic lanthanide complexes as PARACEST agents for medical imaging. *Chem. Soc. Rev.* **2006**, *35*, 500–511. (e) Zhang, S.; Merritt, M.; Woessner, D. E.; Lenkinski, R. E.; Sherry, A. D. PARACEST Agents: Modulating MRI Contrast via Water Proton Exchange. *Acc. Chem. Res.* **2003**, *36*, 783–790. (f) Zhang, S.; Trokowsky, R.; Sherry, A. D. A Paramagnetic CEST Agent for Imaging Glucose by MRI. *J. Am. Chem. Soc.* **2003**, *125*, 15288–15289.
- (12) Liu, G.; Song, X.; Chan, K. W. Y.; McMahon, M. T. Nuts and bolts of chemical exchange saturation transfer MRI. *NMR Biomed.* **2013**, *26*, 810–828.
- (13) (a) Bar-Shir, A.; Liu, G.; Greenberg, M. M.; Bulte, J. W. M.; Gilad, A. A. Synthesis of a probe for monitoring HSV1-tk reporter gene expression using chemical exchange saturation transfer MRI. *Nat. Protoc.* **2013**, *8*, 2380–2391. (b) Bar-Shir, A.; Liu, G.; Liang, Y.; Yadav, N. N.; McMahon, M. T.; Walczak, P.; Nimmagadda, S.; Pomper, M. G.; Tallman, K. A.; Greenberg, M. M.; et al. Transforming Thymidine into a Magnetic Resonance Imaging Probe for Monitoring Gene Expression. *J. Am. Chem. Soc.* **2013**, *135*, 1617–1624. (c) Chan, K. W.; Yu, T.; Qiao, Y.; Liu, Q.; Yang, M.; Patel, H.; Liu, G.; Kinzler, K. W.; Vogelstein, B.; Bulte, J. W.; et al. A diaCEST MRI approach for monitoring liposomal accumulation in tumors. *J. Control. Release* **2014**, *180*, 51–59. (d) Chan, K. W. Y.; Liu, G.; Song, X.; Kim, H.; Yu, T.; Arifin, D. R.; Gilad, A. A.; Hanes, J.; Walczak, P.; van Zijl, P. C. M.; et al. MRI-detectable pH nanosensors incorporated into hydrogels for in vivo sensing of transplanted-cell viability. *Nat. Mater.* **2013**, *12*, 268–275. (e) Haris, M.; Singh, A.; Cai, K.; Nath, K.; Crescenzi, R.; Kogan, F.; Hariharan, H.; Reddy, R. MICEST: a potential tool for non-invasive detection of molecular changes in Alzheimer's disease. *J. Neurosci. Methods* **2013**, *212*, 87–93. (f) Liu, G.; Moake, M.; Har-el, Y.-e.; Long, C. M.; Chan, K. W. Y.; Cardona, A.; Jamil, M.; Walczak, P.; Gilad, A. A.; Sgouros, G.; et al. In vivo multicolor molecular MR imaging using diamagnetic chemical exchange saturation transfer liposomes. *Magn. Reson. Med.* **2012**, *67*, 1106–1113.
- (14) (a) Chan, K. W. Y.; McMahon, M. T.; Kato, Y.; Liu, G.; Bulte, J. W. M.; Bhujwala, Z. M.; Artemov, D.; van Zijl, P. C. M. Natural D-glucose as a biodegradable MRI contrast agent for detecting cancer. *Magn. Reson. Med.* **2012**, *68*, 1764–1773. (b) Walker-Samuel, S.; Ramasawmy, R.; Torrealdea, F.; Rega, M.; Rajkumar, V.; Johnson, S. P.; Richardson, S.; Gonçalves, M.; Parkes, H. G.; Årstad, E.; et al. In vivo imaging of glucose uptake and metabolism in tumors. *Nat. Med.* **2013**, *19*, 1067–1072.
- (15) van Zijl, P. C.; Jones, C. K.; Ren, J.; Malloy, C. R.; Sherry, A. D. MRI detection of glycogen in vivo by using chemical exchange saturation transfer imaging (glycoCEST). *Proc. Natl. Acad. Sci. U.S.A.* **2007**, *104*, 4359–4364.
- (16) Ling, W.; Regatte, R. R.; Navon, G.; Jerschow, A. Assessment of glycosaminoglycan concentration in vivo by chemical exchange-dependent saturation transfer (gagCEST). *Proc. Natl. Acad. Sci. U.S.A.* **2008**, *105*, 2266.
- (17) Bar-Shir, A.; Liu, G.; Chan, K. W. Y.; Oskolkov, N.; Song, X.; Yadav, N. N.; Walczak, P.; McMahon, M. T.; van Zijl, P. C. M.; Bulte, J. W. M.; et al. Human protamine-1 as an MRI reporter gene based on chemical exchange. *ACS Chem. Biol.* **2014**, *9*, 134–138.
- (18) Cai, K.; Haris, M.; Singh, A.; Kogan, F.; Greenberg, J. H.; Hariharan, H.; Dettre, J. A.; Reddy, R. Magnetic resonance imaging of glutamate. *Nat. Med.* **2012**, *18*, 302–306.
- (19) Shin, S. H.; Wendland, M. F.; Zhang, B.; Tran, A.; Tang, A.; Vandsburger, M. H. Noninvasive imaging of renal urea handling by CEST-MRI. *Magn. Reson. Med.* **2020**, *83*, 1034–1044.
- (20) Snoussi, K.; Bulte, J. W.; Guéron, M.; van Zijl, P. C. Sensitive CEST agents based on nucleic acid imino proton exchange: detection of poly(rU) and of a dendrimer-poly(rU) model for nucleic acid delivery and pharmacology. *Magn. Reson. Med.* **2003**, *49*, 998–1005.
- (21) Gilad, A. A.; Bar-Shir, A.; Bricco, A. R.; Mohanta, Z.; McMahon, M. T. Protein and peptide engineering for chemical exchange saturation transfer imaging in the age of synthetic biology. *NMR Biomed.* **2022**, No. e4712.
- (22) Chakraborty, S.; Perucheralathan, S.; Ghosh, A. Paracetamol and other acetanilide analogs as inter-molecular hydrogen bonding assisted diamagnetic CEST MRI contrast agents. *RSC Adv.* **2021**, *11*, 6526–6534.
- (23) Chen, Z.; Han, Z.; Liu, G. Repurposing Clinical Agents for Chemical Exchange Saturation Transfer Magnetic Resonance Imaging: Current Status and Future Perspectives. *Pharmaceuticals* **2021**, *14*, 11.
- (24) (a) Yang, X.; Song, X.; Li, Y.; Liu, G.; Ray Banerjee, S.; Pomper, M. G.; McMahon, M. T. Salicylic Acid and Analogues as diaCEST MRI Contrast Agents with Highly Shifted Exchangeable Proton Frequencies. *Angew. Chem., Int. Ed.* **2013**, *52*, 8116–8119. (b) Lesniak, W. G.; Oskolkov, N.; Song, X.; Lal, B.; Yang, X.; Pomper, M.; Laterra, J.; Nimmagadda, S.; McMahon, M. T. Salicylic Acid Conjugated Dendrimers Are a Tunable, High Performance CEST MRI NanoPlatform. *Nano Lett.* **2016**, *16*, 2248–2253.
- (25) Yang, X.; Yadav, N. N.; Song, X.; Ray Banerjee, S.; Edelman, H.; Minn, I.; van Zijl, P. C. M.; Pomper, M. G.; McMahon, M. T. Tuning Phenols with Intra-Molecular Bond Shifted Hydrogens (IM-SHY) as diaCEST MRI Contrast Agents. *Chem. - Eur. J.* **2014**, *20*, 15824–15832.
- (26) Pandey, S.; Chakraborty, S.; Ghosh, R.; Radhakrishnan, D.; Perucheralathan, S.; Ghosh, A. The role of hydrogen bonding in tuning CEST contrast efficiency: a comparative study of intra- and inter-molecular hydrogen bonding. *New J. Chem.* **2022**, *46*, 1260–1266.
- (27) (a) Zhang, X.; Yuan, Y.; Li, S.; Zeng, Q.; Guo, Q.; Liu, N.; Yang, M.; Yang, Y.; Liu, M.; McMahon, M. T.; et al. Free-base porphyrins as CEST MRI contrast agents with highly upfield shifted labile protons. *Magn. Reson. Med.* **2019**, *82*, 577–585. (b) Chakraborty, S.; Das, M.; Srinivasan, A.; Ghosh, A. Tetrakis-(N-methyl-4-pyridinium)-porphyrin as a diamagnetic chemical exchange saturation transfer (diaCEST) MRI contrast agent. *New J. Chem.* **2021**, *45*, 1262–1268.
- (28) (a) Longo, D. L.; Dastrù, W.; Digilio, G.; Keupp, J.; Langereis, S.; Lanzardo, S.; Prestigio, S.; Steinbach, O.; Terreno, E.; Uggeri, F.; et al. Iopamidol as a responsive MRI-chemical exchange saturation transfer contrast agent for pH mapping of kidneys: In vivo studies in mice at 7 T. *Magn. Reson. Med.* **2011**, *65*, 202–211. (b) Aime, S.; Calabi, L.; Biondi, L.; De Miranda, M.; Ghelli, S.; Paleari, L.; Rebaudengo, C.; Terreno, E. Iopamidol: Exploring the potential use of a well-established x-ray contrast agent for MRI. *Magn. Reson. Med.* **2005**, *53*, 830–834.
- (29) Zhang, S.; Zhou, K.; Huang, G.; Takahashi, M.; Dean Sherry, A.; Gao, J. A novel class of polymeric pH-responsive MRI CEST agents. *Chem. Commun.* **2013**, *49*, 6418–6420.
- (30) (a) Zeng, Q.; Shao, D.; He, X.; Ren, Z.; Ji, W.; Shan, C.; Qu, S.; Li, J.; Chen, L.; Li, Q. Carbon dots as a trackable drug delivery carrier for localized cancer therapy in vivo. *J. Mater. Chem. B* **2016**, *4*, 5119–5126. (b) Azam, N.; Najabat Ali, M.; Javid Khan, T. Carbon Quantum Dots for Biomedical Applications: Review and Analysis. *Front. Mater.* **2021**, *8*, 700403. (c) Murthy, S. K. Nanoparticles in modern medicine: state of the art and future challenges. *Int. J. Nanomed.* **2007**, *2*, 129–141.
- (31) Kombala, C. J.; Kotrotsou, A.; Schuler, F. W.; de la Cerda, J.; Ma, J. C.; Zhang, S.; Pagel, M. D. Development of a Nanoscale Chemical Exchange Saturation Transfer Magnetic Resonance Imaging Contrast Agent That Measures pH. *ACS Nano* **2021**, *15*, 20678–20688.

(32) (a) Li, H.; He, X.; Kang, Z.; Huang, H.; Liu, Y.; Liu, J.; Lian, S.; Tsang, C. H. A.; Yang, X.; Lee, S.-T. Water-Soluble Fluorescent Carbon Quantum Dots and Photocatalyst Design. *Angew. Chem., Int. Ed.* **2010**, *49*, 4430–4434. (b) Liu, M. L.; Chen, B. B.; Li, C. M.; Huang, C. Z. Carbon dots: synthesis, formation mechanism, fluorescence origin and sensing applications. *Green Chem.* **2019**, *21*, 449–471. (c) Wang, X.; Feng, Y.; Dong, P.; Huang, J. A Mini Review on Carbon Quantum Dots: Preparation, Properties, and Electrocatalytic Application. *Front. Chem.* **2019**, *7*, 671.

(33) Zhang, J.; Yuan, Y.; Gao, M.; Han, Z.; Chu, C.; Li, Y.; van Zijl, P. C. M.; Ying, M.; Bulte, J. W. M.; Liu, G. Carbon Dots as a New Class of Diamagnetic Chemical Exchange Saturation Transfer (diaCEST) MRI Contrast Agents. *Angew. Chem., Int. Ed.* **2019**, *58*, 9871–9875.

(34) Dixon, W. T.; Ren, J.; Lubag, A. J. M.; Ratnakar, J.; Vinogradov, E.; Hancu, I.; Lenkinski, R. E.; Sherry, A. D. A concentration-independent method to measure exchange rates in PARACEST agents. *Magn. Reson. Med.* **2010**, *63*, 625–632.

(35) Brandis, K. Alkalinisation of local anaesthetic solutions. *Aust. Prescr.* **2011**, *34*, 173–175.

(36) Carbonaro, C. M.; Corpino, R.; Salis, M.; Mocci, F.; Thakkar, S. V.; Olla, C.; Ricci, P. C. On the Emission Properties of Carbon Dots: Reviewing Data and Discussing Models. *C* **2019**, *5*, 60.